

A Superparamagnetic State Induced by a Spin Reorientation Transition in Ultrathin Magnetic Films

Yousuke NORIZUKI and Munetaka SASAKI

Department of Applied Physics, Tohoku University, Sendai 980-8579

We investigate a spin reorientation transition (SRT) in ultrathin magnetic films by Monte-Carlo simulations. We assume that the lateral size of the film is relatively small and it has a single-domain structure. To gain insights into the SRT, we measure a free-energy as a function of perpendicular and in-plane magnetizations. As a result, we find that the system is in a *superparamagnetic state* at the SRT temperature. The disappearance of magnetization around the SRT temperature, which is observed in experiments, emerges due to dynamical fluctuations in magnetization which are inherent in the superparamagnetic state. This observation is in contrast to that in large ultrathin magnetic films that the disappearance of magnetization is caused by a static magnetic structure with many complex domains.

KEYWORDS: spin reorientation transition, ultrathin magnetic film, Monte-Carlo simulation

In the last several decades, ultrathin magnetic films have studied extensively due to both the fundamental interest of low-dimensional magnetism and the numerous perspectives of applications. These studies have revealed that complex magnetic order and curious phenomena are induced in ultrathin magnetic films by competition among several interactions such as ferromagnetic exchange interactions, magnetic anisotropy energies, and magnetic dipolar interactions. A spin reorientation transition¹⁻⁵⁾ (SRT) is one of such phenomena. This is a transition from a in-plane magnetized state to a perpendicularly magnetized state. This transition is induced by decreasing the thickness of the film or by decreasing the temperature. The SRT has been extensively investigated both experimentally and theoretically until now (see reviews 6, 7 and references therein).

The main issue we address in the present study is the disappearance of magnetization around the SRT temperature T_{SRT} .^{1,4)} This abrupt drop in magnetization around T_{SRT} is called *pseudogap*.⁴⁾ Papas *et al.* proposed that there are two possible origins which cause this pseudogap. The first is a dynamical origin that the system is in a paramagnetic state because perpendicular and in-plane anisotropies compensate with each other around T_{SRT} . As a result, magnetization heavily fluctuates with time, and the time average of each component of magnetization, which is measured in experiments, becomes zero. The second is a static origin that complex magnetic domains, which cause an almost complete loss in the total magnetization of the sample, emerge in the vicinity of T_{SRT} . For large ultrathin films with the lateral size of several tens of micrometers, it was observed that a complex domain structure appears near the SRT temperature.^{3,5)} Such behavior was also observed in Monte-Carlo (MC) study⁸⁾ if the corresponding system size is large enough.⁹⁾ These results strongly indicate that the pseudogap is caused by the static origin for large films. However, it has not been clarified whether the pseudogap emerges due to the dynamical origin even if the lateral size of the film is not large and the system has a single-domain structure.

To address this issue, we examine the SRT of ultrathin magnetic films with focusing on the pseudogap around T_{SRT} . The corresponding size of the film is chosen to be relatively

small so that the system has a single-domain structure. To gain insights into the properties of the SRT, we measure a free-energy as a function of the two order parameters of the SRT, i.e., perpendicular magnetization m_{\perp} and in-plane magnetization m_{\parallel} . To our knowledge, this is the first time that such free-energy is measured in the study of the SRT. The free-energy is calculated numerically by using the method proposed in ref. 10. As a result, we found that the free-energy around T_{SRT} has a structure that low free-energy region widely spreads in the $(m_{\perp}, m_{\parallel})$ space. Because the amplitude of the magnetization $m \equiv (m_{\perp}^2 + m_{\parallel}^2)^{1/2}$ is non-zero in the low free-energy region, spins are aligned in the same direction. However, the direction of the magnetization heavily fluctuates with time as a result of the exploration inside the low free-energy region. In short, the system is in a *superparamagnetic state* at T_{SRT} . Our results indicate that the pseudogap emerges due to the dynamical origin even in relatively small ultrathin magnetic films with a single-domain structure.

In the present work, we consider a spin model on a $32 \times 32 \times 1$ square lattice with open boundaries. The Hamiltonian of the model is described as

$$\mathcal{H} = -J \sum_{\langle i,j \rangle} \mathbf{S}_i \cdot \mathbf{S}_j + C_d \sum_{i < j} \left(\frac{\mathbf{S}_i \cdot \mathbf{S}_j}{r_{ij}^3} - 3 \frac{(\mathbf{S}_i - \mathbf{r}_{ij})(\mathbf{S}_j - \mathbf{r}_{ij})}{r_{ij}^5} \right) - C_u \sum_i (S_i^z)^2, \quad (1)$$

where \mathbf{S}_i is a classical Heisenberg spin with an absolute value of unity, $\mathbf{r}_{ij} \equiv \mathbf{r}_i - \mathbf{r}_j$, \mathbf{r}_i is the position vector of a site i in the unit of the lattice constant, and $r_{ij} \equiv |\mathbf{r}_{ij}|$. In the right hand side of eq. (1), the first term, the second term, and the third term denote ferromagnetic exchange interactions, dipolar interactions, and magnetic anisotropy energies, respectively. The sum of exchange interactions runs over all of the nearest-neighboring pairs. We assume that magnetic anisotropy is uniaxial and its easy axis is parallel to the z -axis, where the z -axis is perpendicular to the film. This type of model has been often used in the study of the SRT.^{8,11-17)}

The three parameters J , C_d , and C_u in eq. (1) represent the strength of each energy term. In the present work, we performed simulations for four different sets of the parameters. The values of C_d/J and C_u/J in the four cases are shown in

Table I. The four sets of parameters used in the present study. The mesh size δ is calculated from eq. (2) and the ratio C_d/J by assuming that $A = 30.2 \times 10^{-12}$ J/m and $J_s = 1.79$ T. The size is calculated from the mesh size δ and the lattice size $32 \times 32 \times 1$.

	C_d/J	C_u/J	δ [nm]	size [nm ³]
case 1	0.007	0.05	1.44	$46.1 \times 46.1 \times 1.44$
case 2	0.028	0.2	2.89	$92.5 \times 92.5 \times 2.89$
case 3	0.056	0.4	4.08	$131 \times 131 \times 4.08$
case 4	0.070	0.5	4.56	$146 \times 146 \times 4.56$

Table I. The ratio C_d/C_u , which is 0.14 in all of the four cases, is chosen so that the SRT is clearly observed. In micromagnetic calculations, the three parameters in eq. (1) are calculated from the material parameters and the mesh size as

$$J = 2\delta A, \quad C_d = J_s^2 \delta^3 / (4\pi\mu_0), \quad C_u = K_u \delta^3, \quad (2)$$

where δ is the mesh size, A is the exchange stiffness constant in continuous limit, J_s is the saturation polarization, K_u is the magnetic anisotropy constant, and μ_0 is the vacuum permeability. The mesh size δ shown in Table I is calculated from the ratio C_d/J by assuming that $A = 30.2 \times 10^{-12}$ J/m and $J_s = 1.79$ T. These values are the same as the material parameters of cobalt,¹⁸⁾ which is one of the representative magnetic materials. The sizes of the film shown in Table I are calculated from the mesh size and the lattice size. The magnetic anisotropy constant K_u is calculated from the ratio $C_d/C_u = 0.14$ as 1.45×10^6 J/m³. Since the magnetic anisotropy constant of cobalt is 4.53×10^5 J/m³,¹⁸⁾ this value is about three times larger than that of cobalt.

We next explain how we measure free-energy as a function of m_\perp and m_\parallel . The free-energy is defined by

$$\exp[-\beta F(\beta; m_\perp, m_\parallel)] \equiv \text{Tr}_{\{\mathbf{S}_i\}} \exp[-\beta \mathcal{H}\{\mathbf{S}_i\}] \times \delta(m_\perp - m_\perp^*\{\mathbf{S}_i\}) \delta(m_\parallel - m_\parallel^*\{\mathbf{S}_i\}), \quad (3)$$

where β is the inverse temperature and $\mathcal{H}\{\mathbf{S}_i\}$ is the Hamiltonian defined by eq. (1). The trace in the right-hand side of eq. (3) runs over all of possible configurations. Note that the right-hand side of the equation is proportional to the probability that spin configurations with magnetizations (m_\perp, m_\parallel) are observed. $m_\perp^*\{\mathbf{S}_i\}$ and $m_\parallel^*\{\mathbf{S}_i\}$ are the perpendicular and in-plane magnetizations calculated from a configuration $\{\mathbf{S}_i\}$, respectively, i.e.,

$$m_\perp^*\{\mathbf{S}_i\} = \frac{1}{N} \left| \sum_i S_i^z \right|, \quad (4)$$

$$m_\parallel^*\{\mathbf{S}_i\} = \frac{1}{N} \sqrt{\left(\sum_i S_i^x \right)^2 + \left(\sum_i S_i^y \right)^2}, \quad (5)$$

where N is the number of spins.

We used the method proposed in ref. 10 to calculate $F(\beta; m_\perp, m_\parallel)$ numerically. In this method, a variant of the Wang-Landau method^{19,20)} is combined with the stochastic cutoff (SCO) method,²¹⁾ which was recently invented for long-range interacting systems. This method enables us to calculate $F(\beta; m_\perp, m_\parallel)$ with reasonable computational time. Furthermore, long-range dipolar interactions are taken into account without any approximations by the use of the SCO method. The detailed conditions of free-energy measurements are as follows. We set the initial value of the modification

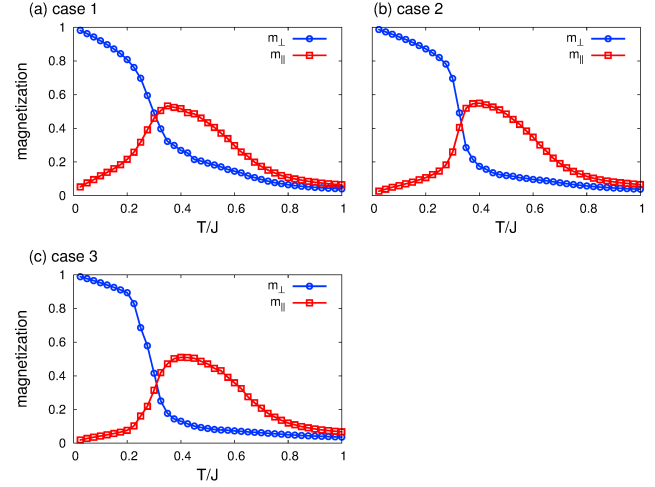


Fig. 1. (Color online) The temperature dependences of the perpendicular magnetization m_\perp (open circles) and in-plane magnetization m_\parallel (open squares) in the case 1 (upper left), 2 (upper right), and 3 (lower left) in Table I. In the measurement, the temperature was gradually cooled from 2.0 J to 0.025 J in steps of $\Delta T = 0.025$ J. The system was kept for 100,000 MC steps at each temperature. The data of the latter 50,000 MC steps were used to calculate the thermal averages of the two magnetizations. The average was also taken over 10 different runs with different initial states and random number sequences.

constant ΔF in ref. 10, which is related with the modification factor f in the Wang-Landau method^{19,20)} by $f = \exp(\Delta F)$, to unity. We stopped our simulation after we halved ΔF 20 times. Therefore, the final ΔF is 2^{-20} . The magnetization space (m_\perp, m_\parallel) was divided into 10,000 bins with the area of 0.01×0.01 , and free-energy was calculated for each bin which satisfies the inequalities $0 \leq (m_\perp^2 + m_\parallel^2)^{1/2} \leq 0.85$. The histogram of two magnetizations $H(m_\perp, m_\parallel)$ was checked every 10,000 MC steps. We regarded the histogram as flat when $H(m_\perp, m_\parallel)$'s for all the magnetizations are not less than 80% of the average value of the histogram. The SCO method was applied only to dipolar interactions. A potential switching procedure in the SCO method was performed every 10 MC steps. We performed the free-energy measurement for 10 different runs with different initial states and random number sequences to estimate the means and errorbars of the free-energy. The estimated error bars were rather small. They were smaller than 0.03 J for all of the data we will show hereafter.

To check whether this model exhibits the SRT or not, we first measured the perpendicular and in-plane magnetizations as a function of the temperature in the three cases 1, 2, and 3 in Table I. Figure 1 shows the result. We hereafter set the Boltzmann constant k_B to unity and use J as a unit of temperature. In this measurement, the temperature was gradually cooled from 2.0 J to 0.025 J in steps of $\Delta T = 0.025$ J, and the thermal averages of the two magnetizations were measured at each temperature. As the temperature decreases, m_\parallel starts to increase rapidly around $T \approx 0.8$ J. On the contrary, such rapid increase does not occur in m_\perp around this temperature. Therefore, m_\parallel is dominant at intermediate temperatures. However, m_\parallel starts to drop around 0.4 J, and m_\perp overtakes m_\parallel around 0.3 J. These data clearly show that the present model exhibits the SRT. We also see that the SRT temperature T_{SRT} , which is defined by the temperature where m_\perp is equal to m_\parallel , is around

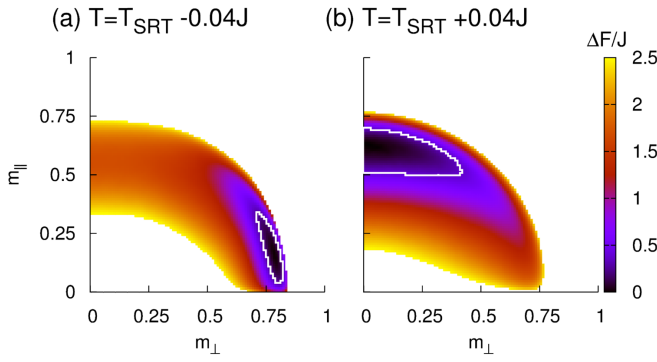


Fig. 2. (Color online) Free-energy difference ΔF in the case 2 is plotted as a function of $(m_{\perp}, m_{\parallel})$ for two different temperatures. ΔF is defined by eq. (6). The left and right panels show the data for $T = T_{\text{SRT}} - 0.04 J$ and those for $T = T_{\text{SRT}} + 0.04 J$, respectively. T_{SRT} is $0.33 J$. In both figures, ΔF is plotted only for a region in which ΔF is smaller than $2.5 J$. The low free-energy region defined by the inequality $\Delta F \leq T$ is denoted by a solid white line. The average was taken over 10 different runs.

$0.3 J$ in all of the three cases. This means that T_{SRT} mainly depends on the ratio C_d/C_u . Recall that the ratio is fixed to 0.14 in all the four cases (see Table I). We also performed MC simulation in the case 4, and found that a two-domain structure emerges in this case. This observation shows that the size in the case 3 is close to the largest size below which a single-domain structure is retained.

One may consider that a pseudogap does not exist in this model because neither m_{\perp} nor m_{\parallel} is zero at T_{SRT} . However, this result is not incompatible with the presence of a pseudogap due to the dynamical origin. It should be recalled that *each component of magnetization* m_{μ} ($\mu = x, y, z$), which can be both positive and negative, disappears at T_{SRT} . When spins are aligned in the same direction and the direction changes with time, the time average of m_{μ} becomes zero. However, the time averages of m_{\perp} and m_{\parallel} do not become zero because they are always positive by definition.

We next measured the free-energy $F(\beta; m_{\perp}, m_{\parallel})$ defined by eq. (3). In Fig. 2, free-energy difference ΔF in the case 2 is plotted as a function of $(m_{\perp}, m_{\parallel})$, where ΔF is defined by

$$\Delta F(\beta; m_{\perp}, m_{\parallel}) \equiv F(\beta; m_{\perp}, m_{\parallel}) - F_{\min}(\beta), \quad (6)$$

and

$$F_{\min}(\beta) \equiv \min_{(m_{\perp}, m_{\parallel})} F(\beta; m_{\perp}, m_{\parallel}). \quad (7)$$

Figures 2(a) and 2(b) show the data for $T < T_{\text{SRT}}$ and those for $T > T_{\text{SRT}}$, respectively. We see that ΔF for $T < T_{\text{SRT}}$ has a global minimum around $(m_{\perp}, m_{\parallel}) \approx (0.75, 0.15)$. In contrast, when $T > T_{\text{SRT}}$, ΔF has a global minimum around $(m_{\perp}, m_{\parallel}) \approx (0, 0.6)$. The location of the global minimum shifts discontinuously as the temperature is changed across T_{SRT} . In this sense, we can regard the SRT as a first-order transition. This discontinuous shift of the global minimum explains the reason why m_{\perp} and m_{\parallel} in Fig. 1 change abruptly around T_{SRT} . This result is consistent with the previous results that single monolayer magnetic films with a single-domain structure exhibit a first-order transition.^{12, 17, 22)} A similar discontinuous shift in the global minimum was observed in the other two cases 1 and 3.

We next focus our attention to the free-energy structure at

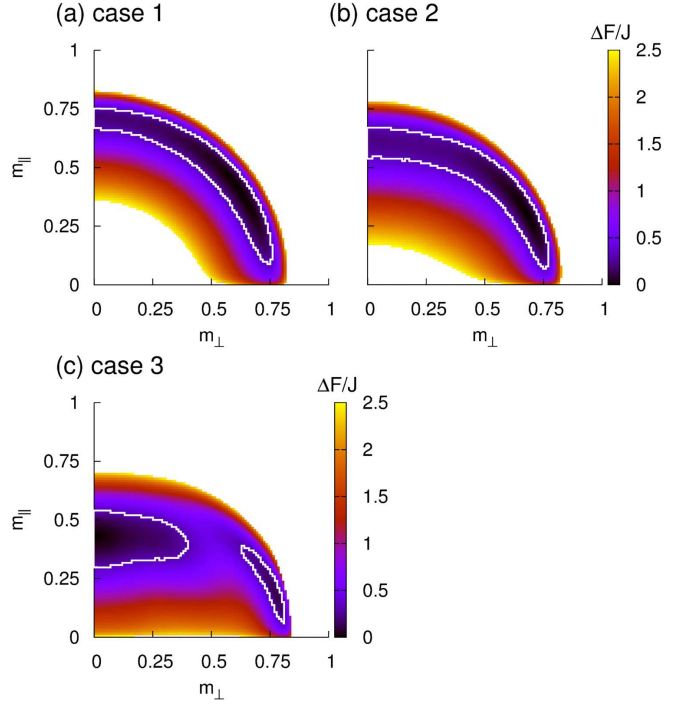


Fig. 3. (Color online) Free-energy difference ΔF at T_{SRT} is plotted as a function of $(m_{\perp}, m_{\parallel})$ for the case 1 (upper left), 2 (upper right), and 3 (lower left). ΔF is plotted only for a region in which ΔF is smaller than $2.5 J$. The low free-energy region defined by the inequality $\Delta F \leq T$ is denoted by a solid white line. The average was taken over 10 different runs.

T_{SRT} . In Fig. 3, we show ΔF for all of the three cases. There are several differences in the free-energy structure among the three cases. When C_d and C_u are small (case 1), the free-energy has a circular structure. In the case 2, this free-energy structure is slightly deformed into an elliptical one. For large C_d and C_u (case 3), the deformation proceeds further, and the free-energy has two local minima and a free-energy barrier in between. However, a common feature among the three free-energy structures is that a low free-energy region defined by the inequality $\Delta F \leq T$, which is denoted by a solid white line in Fig. 3, widely spreads in the $(m_{\perp}, m_{\parallel})$ space. In the cases 1 and 2, low free-energy region involves both the perpendicularly magnetized state with $m_{\parallel} \approx 0$ and the in-plane magnetized state with $m_{\perp} \approx 0$. There is no (or vanishingly small) barrier between the two states. In the case 3, there is a free-energy barrier like an ordinary first-order phase transition. However, the barrier is rather small. Therefore, we can expect that magnetization at T_{SRT} heavily fluctuates with time.

To verify whether this reasoning is correct or not, we performed a standard MC simulation at T_{SRT} and measured the amplitude of magnetization $m \equiv (m_{\perp}^2 + m_{\parallel}^2)^{1/2}$ and the z -component of magnetization m_z . Figure 4 shows the result. The data in the case 1 and those in the case 3 are shown in Figs. 4(a) and 4(b), respectively. We see that m_z 's in both the cases heavily fluctuate with time, as expected. A similar behavior was observed in the other two components of magnetization m_x and m_y . However, the amplitude of magnetization m is always non-zero because m is non-zero in the low free-energy region of ΔF . Especially, in the case 1, m in the low free-energy region is almost constant because ΔF has a circular structure. This is the reason why fluctuations in m are

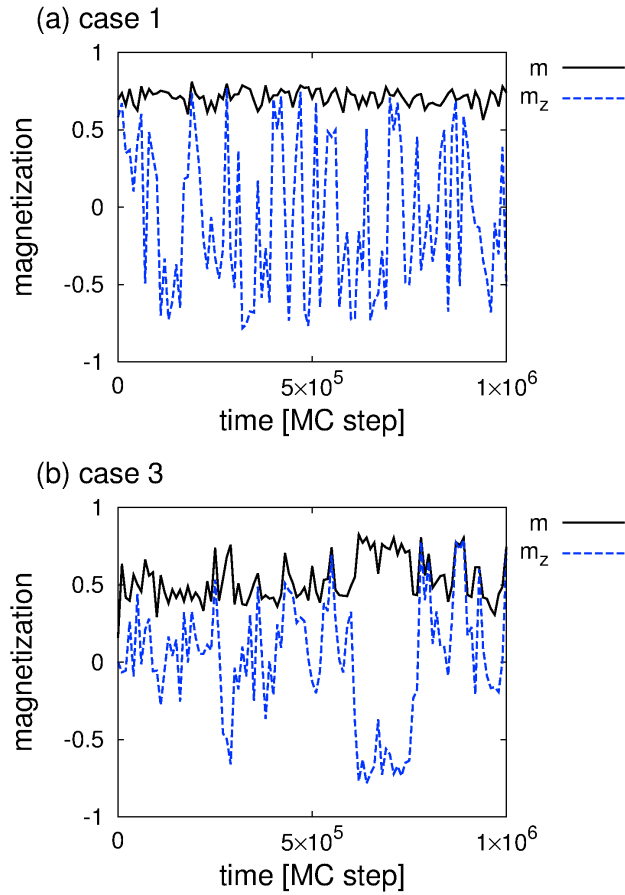


Fig. 4. (Color online) The amplitude of magnetization $m \equiv (m_x^2 + m_y^2)^{1/2}$ and the z-component of magnetization m_z measured at T_{SRT} are plotted as a function of time for the two cases 1 (upper panel) and 3 (lower panel).

rather small in the case 1. These results show that, at the SRT temperature, spins are aligned in the same direction, and the direction changes with time. In other words, the system is in a superparamagnetic state at T_{SRT} . Therefore, the pseudogap in magnetization emerges around the SRT temperature because of dynamical fluctuations in magnetization which are inherent in the superparamagnetic state.

In conclusion, we investigated the spin reorientation transition (SRT) in ultrathin magnetic films by Monte-Carlo simulations. We concentrated ourselves on the case that the lateral size of the film is relatively small and the system has a single-domain structure. As a result of free-energy measurement, we

found that the system is in a superparamagnetic state at T_{SRT} and the disappearance (pseudogap) of magnetization around T_{SRT} emerges due to dynamical fluctuations in magnetization. This observation is in contrast to that in large ultrathin magnetic films that the pseudogap is caused by a static magnetic structure with many complex domains.

Acknowledgment

The authors would like to thank Professor K. Sasaki for valuable discussions and comments.

- 1) D. P. Papas, K.-P. Kämper, and H. Hopster: Phys. Rev. Lett. **64** (1990) 3179.
- 2) R. Allenspach, M. Stampanoni, and A. Bischof: Phys. Rev. Lett. **65** (1990) 3344.
- 3) R. Allenspach and A. Bischof: Phys. Rev. Lett. **69** (1992) 3385.
- 4) Z. Q. Qiu, J. Pearson, and S. D. Bader: Phys. Rev. Lett. **70** (1993) 1006.
- 5) M. Speckmann, H. P. Oepen, and H. Ibach: Phys. Rev. Lett. **75** (1995) 2035.
- 6) K. De'Bell, A. B. MacIsaac, and J. P. Whitehead: Rev. Mod. Phys. **72** (2000) 225.
- 7) P. J. Jensen and K. H. Bennemann: Surf. Sci. Rep. **61** (2006) 129.
- 8) M. Carubelli, O. V. Billoni, S. A. Pighin, S. A. Cannas, D. A. Stariolo, and F. A. Tamarit: Phys. Rev. B **77** (2008) 134417.
- 9) In ref. 8, the authors used the same Hamiltonian as eq. (1) and set the ratio C_d/J to be 0.33. By assuming that the material parameters A and J_s are the same as those used in the calculation shown in Table I, the mesh size δ is calculated to be about 10 nm from eq. (2) and the ratio C_d/J . Because the lattice size is $40 \times 40 \times 1$, the corresponding system size is estimated to be $400 \text{ nm} \times 400 \text{ nm} \times 10 \text{ nm}$.
- 10) K. Watanabe and M. Sasaki: J. Phys. Soc. Jpn. **80** (2011) 093001.
- 11) S. T. Chui: Phys. Rev. B **50** (1994) 12559.
- 12) A. Hucht, A. Moschel, and K. D. Usadel: J. Magn. Magn. Mater. **148** (1995) 32.
- 13) A. B. MacIsaac, K. De'Bell, and J. P. Whitehead: Phys. Rev. Lett. **80** (1998) 616.
- 14) E. Y. Vedmedenko, A. Ghazali, and J. C. Lévy: Phys. Rev. B **59** (1999) 3329.
- 15) E. Y. Vedmedenko, H. P. Oepen, A. Ghazali, J. C. Lévy, and J. Kirschner: Phys. Rev. Lett. **84** (2000) 5884.
- 16) E. Y. Vedmedenko, H. P. Oepen, and J. Kirschner: Phys. Rev. B **66** (2002) 214401.
- 17) C. Santamaria and H. T. Diep: J. Magn. Magn. Mater. **212** (2000) 23.
- 18) H. Kronmüller and M. Fähnle: *Micromagnetism and the Microstructure of Ferromagnetic Solids* (Cambridge University Press, Cambridge, 2003), Chapter 2.
- 19) F. Wang and D. P. Landau: Phys. Rev. Lett. **86** (2001) 2050.
- 20) F. Wang and D. P. Landau: Phys. Rev. E **64** (2001) 056101.
- 21) M. Sasaki and F. Matsubara: J. Phys. Soc. Jpn. **77** (2008) 024004.
- 22) A. Moschel and K. D. Usadel: Phys. Rev. B **51** (1995) 16111.